8-4-2016

Design maps for fracture resistant functionally graded materials

Muhammad Ridwan Murshed
Rowan University

DESIGN MAPS FOR FRACTURE RESISTANT FUNCTIONALLY GRADED MATERIALS

by
Muhammad Ridwan Murshed

A Thesis

Submitted to the
Department of Mechanical Engineering
College of Engineering
In partial fulfillment of the requirement
For the degree of
Master of Science in Mechanical Engineering
at
Rowan University
April 4, 2016

Thesis Chair: Shivakumar I. Ranganathan, Ph.D.

Dedications

I would like to dedicate this manuscript to my parents.

Acknowledgements

First and foremost, I would like to thank my advisor Professor Shivakumar I. Ranganathan for his words of encouragement, continued patience, constant guidance and invaluable insights that helped me complete this thesis. He pushed me to my limits and gave me a chance to envision a bright future as an independent researcher. I will remain highly indebted to him for his ever-lasting support during difficult times which made this experience a rewarding and an enriching one.

I wish to express my sincere gratitude to Professor Farid H. Abed for his constructive suggestions and technical assistance in order to enhance the quality of this research. I would also like to thank Professors James A. Nemes and Tirupathi R. Chandrupatla for serving on my thesis committee and for their positive inputs on my research.

I am grateful to Professor Jennifer A. Kadlowec for her guidance and support during the course of my studies. Special thanks to the Department of Mechanical Engineering at Rowan for giving me this invaluable opportunity to widen my horizon of knowledge. I would also like to thank the support staff of College of Engineering, namely Barbara K. Wynn and Jessica L. Lee for assisting me with various other matters.

I am extremely thankful to all my friends who have constantly supported me throughout this journey and encouraged me to pursue my dreams and ambitions.

Finally, I take this opportunity to thank my parents and my brother for believing in me when it mattered most. I will forever remain grateful to them for their undying love and support.

Abstract

Muhammad Ridwan Murshed
DESIGN MAPS FOR FRACTURE RESISTANT FUNCTIONALLY GRADED MATERIALS
2015-2016
Shivakumar I. Ranganathan, Ph.D.
Master of Science in Mechanical Engineering

The objective of this research is to generate design maps to identify functionally graded microstructures with enhanced fracture toughness. Several Functionally Graded Materials (FGMs) with an edge crack and membrane loading are considered and the resulting J-integral values are computed numerically using Finite Element Analysis. In order to capture the resulting stress fields accurately, Barsoum elements are used in the vicinity of the crack tip and the simulations are carried out for several crack lengths (a) and material contrasts (κ). The averages of the J-integral values are used to determine the normalized Stress Intensity Factors which are then benchmarked with existing analytical solutions in special cases. Furthermore, in order to facilitate an objective comparison between FGMs and homogeneous materials, a constraint is imposed on each of the microstructure so that the volume averaged modulus remains the same although the spatial variation is very different. Subsequently, we demonstrate that a FGM could perform either better or worse than the reference homogeneous material depending upon the crack length, the type of functional gradation and the material contrast (thereby the local gradient of the modulus at the crack tip). Finally, the notion of 'Fracture Index' is introduced using which 'design maps' are created in the $(a - \kappa)$ space that reveal microstructures with enhanced fracture resistance. These maps are universal since any Functionally Graded Material can be mapped as a point on this space.

Table of Contents

List of Figures

List of Tables

Table Page

Chapter 1

Introduction

Functionally Graded Materials are a subset of inhomogeneous materials and have unique mechanical, thermal and electrical properties due to the controlled spatial variation of material properties. This is in contrast to several homogeneous materials that typically have lower structural integrity when compared to their FGM counterparts. In fact, inhomogeneous materials are ubiquitous in nature and most materials exhibit some form of inhomogeneity when considered at appropriate length scales. Functionally Graded Materials have been found to be useful in several applications in engineering and medicine. For instance, FGMs have been used for synthesizing thermal barrier coating for space applications [1, 2], design of columns [3, 4], piezoelectric and thermoelectric devices [5, 6] and in dental implants which have demonstrated superior mechanical behavior, biocompatibility and osseointegration improvement [7, 8]. Also, with the advent of additive manufacturing, functionally graded bone implants with superior fracture resistance can be printed in a cost-effective manner [9, 10]. It is therefore imperative to understand the behavior of FGMs in order to effectively design composites for target applications.

In the past, several techniques have been used to examine the fracture of FGMs and some of these are noteworthy. Gibson [11] laid the foundation for analyzing FGMs by modeling soil as a heterogeneous material. In the study, the author examines an elastic half space in which the Young's Modulus, E is varied with depth. Analytical and semi-analytical approaches were subsequently used by Delale and Erdogan [12], Erdogan and Wu [13] and Chan et al. [14] in order to investigate cracks in heterogeneous materials. In particular, Delale and Erdogan [12] derive the integral equation for mode-I loading and prove that the Poisson's ratio, v has a

negligible impact on the Stress Intensity Factor (SIF). By exponentially varying the Young's Modulus in the direction parallel to the crack, the authors demonstrate that the crack surface displacement is lower in the stiffer portion of the heterogeneous material as compared to the homogeneous material and vice-versa. Along similar lines, Erdogan and Wu [13] analyze a FGM that has a crack perpendicular to the boundaries. The Young's Modulus is varied along the thickness of the material in order to obtain the results under various loadings such as fixed grip, membrane and bending. The mode-I SIF is obtained for edge cracks and it is seen that the inhomogeneity in the material directly impacts the stress distribution and the SIF. For membrane and bending loadings, the SIF is higher for lower material contrasts and is lower for higher material contrasts. This is in contrast to fixed grip loadings where the trend is vice-versa.

Chan et al. [14] employ a numerical approach for analyzing the mode-III crack problem. A displacement based integral equation is transformed into a hyper singular integral equation that has a varying Shear Modulus, G. The authors highlight that the normalized SIF is independent of Shear Modulus for a homogeneous material. On the contrary, the SIF is inversely proportional to the Shear Modulus in a heterogeneous material. The results using displacement based approach for normalized SIF on the inhomogeneous material are compared with the slope based approach (analytical solution). The results are in good agreement with each other and it is concluded that the displacement based method could be used to replace the integral method.

An alternate approach to analyze fracture using Extended Finite Element Method (XFEM) was proposed by Dolbow and Gosz [15]. In their work, a novel approach was used for computing the mixed mode SIF at the crack tip of FGMs. This involved employing the interaction energy contour integral and representing it as a domain integral which was later used in the XFEM analysis. The authors

observed that for an edge crack, an increase in the material gradation decreased both the mode-I and mode-II normalized SIF.

Rao and Rahman [16] used the Element Free Galerkin's Method (EFGM) to obtain the SIF for a 2D stationary crack in a heterogeneous medium. The material parameters were spatially varied as smooth functions and several integral equations were obtained for analyzing mixed mode fracture. Five problems were taken into consideration and the results obtained for mode-I and mixed mode fracture were compared with analytical as well as numerical solutions. It was seen that EFGM results were in good agreement with the reference solutions.

Several authors have also employed numerical simulations based on Finite Element Method (FEM) to model fracture in FGMs. In particular, Eischen [17] developed equations for analyzing energy release rates and mixed mode SIF of heterogeneous materials using an extended version of the Williams eigenfunction expansion technique. This path-independent integral was juxtaposed with FEM and a composite strip was analyzed with a hyperbolic tangential variation of the Young's Modulus. The author proved that the SIF gradually increased with an increase in the heterogeneous parameter and was always bounded. This is in contrast to the analytical results which demonstrated that the SIF was unbounded for a specific crack length. Along similar lines, Kim and Paulino [18] examined stationary cracks in a FGM and varied the elastic moduli as a smooth function of spatial coordinates. This was then incorporated into the stiffness matrix and the SIF for mode-I along with mixed mode cases were compared using three new approaches for analyzing fracture: i) path independent J-integral method for inhomogeneous materials; ii) modified crack-closure integral method (MCC); iii) displacement correlation technique (DCT). The authors concluded that for mode-I case, the solution obtained using any of these three approaches were identical.

Gu et al. [19] demonstrated a Finite Element based method for obtaining SIF of FGMs using the J-integral method for mode-I fracture. In their study, the authors proved that the second term in the domain integral equation that captured the inhomogeneity in FGMs was negligible as compared to the first term which was the standard domain integral. As a result, the domain integral equation could be evaluated around the crack tip by mesh refinement. Thus, the SIF for FGMs were obtained without taking the material gradient into consideration. Similarly, Gu and Asaro [20] considered the problem of a semi-infinite crack in a FGM strip that was subjected to edge loading. Also, in plane deformation was modeled in order to analytically examine the mixed mode SIF. The authors determined that the material gradation directly impacted the SIF and specifically the mode-II SIF played a major role in the fracture of FGMs. In addition, FGMs were able to withstand higher loadings as compared to their homogeneous counterparts.

Bao and Wang [21] illustrated the use of a FGM that consisted of ceramic and metal layers. This was a linearly elastic FGM in which the Young's Modulus varied throughout the thickness of the film. In order to study the effects of mechanical and thermal loadings on the functionally graded coating, Finite Element Analysis was carried out using ABAQUS. The authors concluded that FGM reduced the Crack Driving Force (CDF) significantly as compared to a ceramic layer when thermal loads were applied. For mechanical loadings, the effect of coating gradation on the CDF was not very high when compared with a ceramic coating. In addition, Bao and Cai [22] examined the delamination cracking phenomena that was observed when thermal expansion led to an imbalance between functionally graded coating and substrate. The thermo-mechanical property of the FGM that consisted of ceramic and metallic layers was varied with respect to the position of the coating along the direction of the thickness. It was observed that the gradation played a major impact on the CDF of the delamination crack by reducing the CDF significantly which would thereby

increase the fracture resistance of the material. In addition, buckling was also studied and the functional gradation led to a decrease in buckling in the delamination crack.

Anlas et al. [23] performed Finite Element Analysis and obtained the J-integral values for a FGM plate with an edge crack in order to calculate SIF. Numerical simulations were carried out using ABAQUS and the domain was discretized into forty parts to model the gradation in the Young's Modulus. Elements consisting of four nodes and four integration points were used for obtaining the results. Further, the authors discussed that the J-integral was path dependent for an inhomogeneous material. However, the value for the J-integral could be used to determine the SIF for a heterogeneous material in the vicinity of the crack tip. Finally, the authors benchmarked their results for uniform traction and uniform displacement loadings and were successful in obtaining accurate results.

More recently, Hossain et al. [24] proposed a new methodology to determine the toughness of a heterogeneous medium that was independent of the details of the boundary condition. Instead, the authors numerically simulated a domain by applying a surfing boundary condition to a steadily growing macroscopic crack. Subsequently, the effective toughness was obtained by using the energy release rate required to propagate the crack.

In summary, a significant amount of literature exists for determining the fracture toughness of FGMs. However, to the best of our knowledge there is no framework to unify the treatment of FGMs in order to identify microstructures that maximize fracture toughness. The notion of 'Fracture Index' and 'design maps' will be introduced in this thesis to fill this void in existing literature. In the subsequent sections, we develop the necessary mathematical models and the resulting boundary value problems are then solved numerically using Finite Element Analysis. The results obtained are first benchmarked with existing solutions for special cases. After

validating the numerical model, the 'Fracture Index' is computed for Functionally Graded Materials as a function of crack length and material contrast. This procedure is repeated for a variety of functional distributions to generate the 'design maps'. It will be demonstrated that these maps highlight the admissible regions for designing microstructures with enhanced fracture resistance.

Chapter 2

Mathematical Background

The J-integral is widely used in order to accurately obtain Stress Intensity Factors (SIFs) at crack tips (see Abd-Elhady and Sallam [25], Aliha et al. [26] and Dancette et al. [27]). It is an alternative to the strain energy release rate and was first proposed by Rice [28] in order to analyze cracks. For Functionally Graded Materials, Delale and Erdogan [12] studied the problem of Mode-I loading with a variation of Young's Modulus in the direction parallel to the crack. The authors stated "it is reasonable to expect that in nonhomogeneous materials with continuous and continuously differentiable elastic constants the nature of the stress singularity at a crack tip would be identical to that of a homogeneous solid". Similarly, Erdogan [29] stated that if a crack was embedded into an inhomogeneous medium with smoothly varying elastic properties, the square root nature of the stress singularity seemed to remain unchanged.

The conjecture by Delale and Erdogan was analytically proven by Eischen [17] using an eigenfunction expansion technique similar to that of Williams [30]. In the study, Eischen considered a constant Poisson's ratio and a general functional form of the Young's Modulus variation. The author proved that a $r^{-\frac{1}{2}}$ stress and strain singularity existed at the crack tip, r being the radial distance measured from the crack tip. In addition, the angular variation of the singular stress field and the associated displacements around a crack tip in a Functionally Graded Material were shown to be exactly the same as the angular variation in a homogeneous material (see Eischen [17] and Honein and Herrmann [31]). With this framework laid out, we will now demonstrate the J-integral in two dimensions and its relation to the Stress Intensity Factor.

In general, the J-integral can be defined as [32, 33]

$$J = \lim_{\Gamma \to 0} \int_{\Gamma} \mathbf{n} \cdot \mathbf{H} \cdot \mathbf{q} d\Gamma \tag{1a}$$

where

$$\mathbf{H} = W\mathbf{I} - \boldsymbol{\sigma} \cdot \frac{\partial \mathbf{u}}{\partial \mathbf{x}} \tag{1b}$$

and Γ is a contour around the crack tip (see Fig. 1), the limit $\Gamma \to 0$ indicates that Γ shrinks onto the crack tip, $\mathbf{q}$ is a unit vector in the virtual crack extension direction, $\mathbf{n}$ is the outward normal to Γ, $\mathbf{I}$ is the Kronecker Delta, W is the strain energy density, $\boldsymbol{\sigma}$ is the stress component and $\mathbf{u}$ is the displacement. Moreover, it has been observed that the J-integral is path dependent around a crack tip in FGMs. However, the J-integral value for a path adjacent to the crack tip in FGMs is identical to that for homogeneous materials as $\Gamma \to 0$. This approach has been employed by various authors such as Gu et al. [19], Anlas et al. [23], Nikbakht and Choupani [34] and Martínez-Pañeda and Gallego [35].

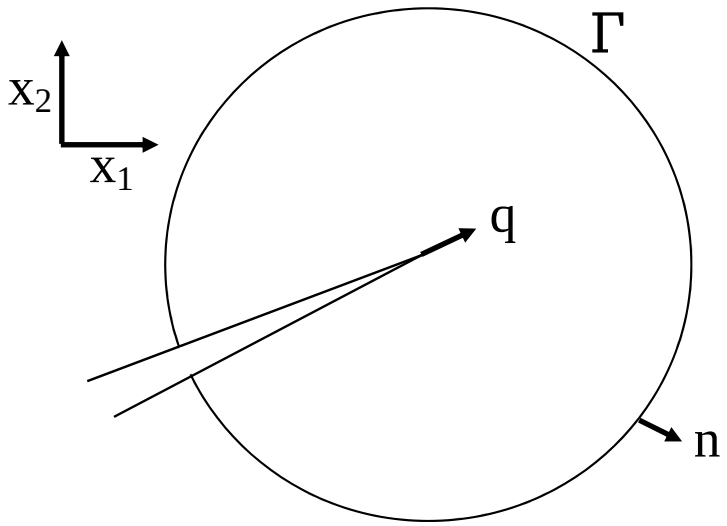

Figure 1: Contour for evaluation of the J-integral

We now illustrate the relation of J-integral with Stress Intensity Factor for a linear elastic material which can be defined as [34, 36]

$$J = \frac{1}{8\pi}\mathbf{K}^T \cdot \mathbf{B}^{-1} \cdot \mathbf{K} \tag{2a}$$

where

$$\mathbf{K} = [K_I, K_{II}, K_{III}]^T \tag{2b}$$

and K_I, K_{II}, K_{III} are the Stress Intensity Factors for mode-I, mode-II and mode-III loadings, respectively. Also, $\mathbf{B}$ is the pre-logarithmic energy factor matrix (see Shih and Asaro [37] and Barnett and Asaro [38]). Now, consider two independent equilibrium states of a cracked body which are actual and auxiliary. The actual state corresponds to the displacement and stress fields for the given boundary conditions. Whereas, the auxiliary state characterizes the displacement and stress fields in the vicinity of the crack tip [16]. The J-integral for the actual state can be defined as [34, 36]

$$\begin{aligned} J = \frac{1}{8\pi}[K_I B_{11}^{-1} K_I + 2K_I B_{12}^{-1} K_{II} + 2K_I B_{13}^{-1} K_{III}] \\ +(terms\ not\ involving\ K_I) \end{aligned} \tag{3}$$

where I, II and III correspond to 1, 2 and 3 when indicating the components of $\mathbf{B}$. Next, the J-integral for an auxiliary state with pure mode-I loading can be seen as [34, 36]

$$J_{aux}^I = \frac{1}{8\pi} k_I \cdot B_{11}^{-1} \cdot k_I \tag{4}$$

where, k_I is the Stress Intensity Factor for the auxiliary state. The superposition of actual Eq. (3) and auxiliary states Eq. (4) results in another equilibrium state for

which the J-integral is expressed as [34, 36]

$$J^I_{tot} = \frac{1}{8\pi}[(K_I + k_I)B^{-1}_{11}(K_I + k_I) + 2(K_I + k_I)B^{-1}_{12}K_{II} + 2(K_I + k_I)B^{-1}_{13}K_{III}] \\ +(terms\ not\ involving\ K_I\ or\ k_I) \tag{5}$$

Now, consider the terms not involving K_I or k_I in J^I_{tot} and J as equal. Using Eqs. (3, 4 & 5) an interaction integral can be defined as [34, 36]

$$J^I_{int} = J^I_{tot} - J - J^I_{aux} = \frac{k_I}{4\pi}(B^{-1}_{11}K_I + B^{-1}_{12}K_{II} + B^{-1}_{13}K_{III}) \tag{6}$$

Moreover, if the calculations are repeated for mode-II and mode-III loadings, the resulting linear system in Eq. (6) can be written as [34, 36]

$$J^\alpha_{int} = \frac{k_\alpha}{4\pi}B^{-1}_{\alpha\beta}K_\beta \tag{7}$$

where, α and β are both I, II and III. Next, Eq. (7) is modified by computing k_α = 1 and the resulting equation is [34, 36]

$$\mathbf{K} = 4\pi\mathbf{B}\cdot\mathbf{J}_{int} \tag{8a}$$

and

$$\mathbf{J}_{int} = [J^I_{int}, J^{II}_{int}, J^{III}_{int}]^T \tag{8b}$$

Here, J^I_{int}, J^{II}_{int} and J^{III}_{int} represents the interaction integrals for mode-I, mode-II and mode-III loadings, respectively. Based on the definition of the J-integral (see Eq. 1a), the interaction integrals J^α_{int} can be expressed as [34, 36]

$$J^\alpha_{int} = \lim_{\Gamma\to 0}\int_\Gamma \mathbf{n}\cdot\mathbf{M}^\alpha\cdot\mathbf{q}d\Gamma \tag{9}$$

where

$$\mathbf{M}^{\alpha} = \boldsymbol{\sigma} : \boldsymbol{\epsilon}^{\alpha}_{aux}\mathbf{I} - \boldsymbol{\sigma} \cdot \left(\frac{\partial \mathbf{u}}{\partial \mathbf{x}}\right)^{\alpha}_{aux} - \boldsymbol{\sigma}^{\alpha}_{aux} \cdot \frac{\partial \mathbf{u}}{\partial \mathbf{x}} \tag{10}$$

Here, $\boldsymbol{\epsilon}$ is the strain component, the subscript aux represents three auxiliary pure Mode I, Mode II, and Mode III crack-tip fields for $\alpha = I, II, III$, respectively. Also, Γ is a contour around the crack tip (see Fig. 1) and the limit $\Gamma \to 0$ indicates that Γ shrinks onto the crack tip.

The interaction integrals, J^{α}_{int} were evaluated using the virtual crack extension technique in 'ABAQUS' (see Fischer et al. [39], Dancette et al. [27] and Aliha et al. [26]). The analysis was carried out by defining the node set along with the number of contours around the crack tip (see Abd-Elhady and Sallam [25] and Bernard et al. [40]). In addition, each contour formed an element set and it consisted of rings of elements surrounding the crack tip (see Abaqus Analysis User's Manual [41], Nikbakht and Choupani [34] and Brocks and Scheider [42]). The element set that formed each ring from the node set was used in order to calculate the J-integral (see Bernard et al. [40]). In the present work, the J-integral values were obtained from second, third and fourth contours (see Fig. 4) and an average J-integral value was used from these contours for calculating the Stress Intensity Factor. This approach has been successfully employed by several other authors including Kamaya [43], Kim et al. [44] and Bayley and Bell [45].

We now illustrate the relation of J-integral with Stress Intensity Factor for a linear elastic material under mode-I loading which can be defined as (see Abd-Elhady and Sallam [25], Shih and Asaro [37] and Barnett and Asaro [38])

$$J = \frac{1}{8\pi} K_I \cdot B_{11}^{-1} \cdot K_I \tag{11a}$$

and

$$B_{11}^{-1} = \frac{8\pi(1-v^2)}{E} \tag{11b}$$

where K_I is the Stress Intensity Factor and v is the Poisson's ratio. Using Eqs. (11a) and (11b), the J integral can be written as [16, 36]

$$J = \frac{K_I^2(1-v^2)}{E} \tag{12}$$

At this stage, it is convenient to illustrate that for Functionally Graded Materials under mode-I loading and plane strain conditions, Eq. (12) can be defined as

$$J = \frac{K_I^2(1-v_{tip}^2)}{E_{tip}} \tag{13}$$

where, E_{tip} and v_{tip} are the Young's Modulus and Poisson's ratio evaluated at the crack tip, respectively (see Rao and Rahman [16], Kim and Paulino [46], Jin and Batra [47] and Yau et al. [48]). Eq. (13) will be employed in this research in order to extract the Stress Intensity Factor for FGMs. In the next section, we will illustrate the methodology to numerically obtain the fracture toughness of Functionally Graded Materials as a function of crack length and material contrast.

Chapter 3

Methodology

The methodology employed in the current study is summarized in Figs. (2a & b). It can be seen that any point on Fig. (2a) reveals the Young's Modulus at that spatial location and the color reveals the contrast for the specific FGM microstructure. Then, 'Fracture Index' is obtained and 'design maps' are created in the $(a-\kappa)$ space that demonstrate regions for constructing microstructures with enhanced fracture resistance (see Fig. 2b).

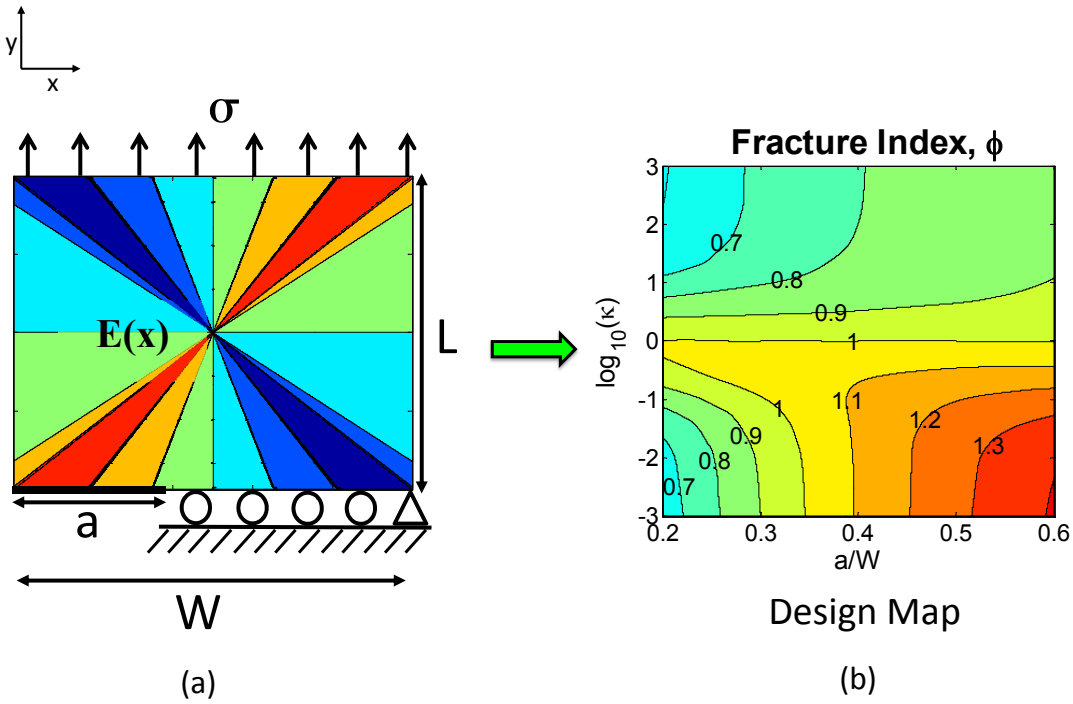

Figure 2: Methodology employed: (a) FGM Strip with Crack Length (a) [The red color indicates high contrast and the blue color indicates low contrast], Width of the Strip (W), Length of the Strip (L), Stress Applied (σ), E(x) which is the linear distribution of Young's Modulus and (b) Design Map with Fracture Index (ϕ), non-dimensional Crack Length ($\frac{a}{W}$) and Material Contrast (κ)

In the present work, several Functionally Graded Materials with an edge crack length (a) and membrane loading are considered and the resulting J-integral

values are obtained numerically using Finite Element Analysis. The averages of the J-integral values are used to determine the normalized Stress Intensity Factors which are then benchmarked with existing analytical solutions in special cases. The procedure is repeated for a variety of crack lengths and material contrasts (κ). Subsequently, the notion of 'Fracture Index' is introduced (see Eq. 20) using which 'design maps' are created in the $(a - \kappa)$ space that highlights the admissible regions for designing fracture resistant materials. In order to objectively compare various functional distributions, all microstructures considered in this study have the same volume averaged Young's Modulus. Based on this constraint, several functionally graded microstructures were created as illustrated in TABLES (1-4). The functions examined were linear, quadratic, exponential and cosine. The linear variation of Young's Modulus is demonstrated in Fig. (3a) and is defined as

$$E(x) = (E_2 - E_1)x + E_1, \qquad (0 \leq x \leq 1) \tag{14}$$

where, E_1 is the Young's Modulus at the left boundary and E_2 is the Young's Modulus at the right boundary. The linear function can also be interpreted as the first two significant terms in a Taylor series expansion of any FGM distribution. Similarly, the quadratic variation of Young's Modulus can be predicted by the first three significant terms in a Taylor series expansion (see Fig. 3b). The quadratic function can be defined as

$$E(x) = (3E_2 + 3E_1 - 6)x^2 + (-2E_2 - 4E_1 + 6)x + E_1, \qquad (0 \leq x \leq 1) \tag{15}$$

The linear and quadratic functions illustrated by Eqs. (14 & 15) have been used in the past by various authors such as Zhong and Cheng [49] and Elishakoff and Guede [50]. Furthermore, an exponential variation of the Young's Modulus is

illustrated in Fig. (3c). Such a distribution has been widely used by several authors such as Erdogan and Wu [13], Rao and Rahman [16] and Guo and Noda [51] and is defined as follows

$$E(x) = E_1 exp[ln(\frac{E_2}{E_1})x], \qquad (0 \leq x \leq 1) \tag{16}$$

Finally, we consider a cosine distribution of Young's Modulus as given in Fig. (3d). This variation was chosen to mimic biological materials such as bone that have hierarchical structure of protein and mineral embedded in layers in order to increase the stiffness and toughness of the bone (see Fratzl et al. [52]). Because a distribution of material properties in a biological material directly leads to a change of the energy consumed by fracture, the cosine function used to examine this phenomenon is

$$E(x) = E_0[1 + \frac{\rho - 1}{\rho + 1} cos(2\pi x)], \qquad (0 \leq x \leq 1) \tag{17}$$

Here, $E_0 = 1$ and $1 \leq \rho \leq 6$. In the next section, these functions will be used in order to study the fracture performance of Functionally Graded Materials.

Table 1: Function used for the gradation-Linear Function:

$$E(x) = (E_2 - E_1)x + E_1$$

Microstructure	E_1 (MPa)	E_2 (MPa)
1	0.001988	1.998
2	0.01980	1.980
3	0.0613	1.939
4	0.1818	1.818
5	0.4805	1.519
6	1	1
7	1.519	0.4805
8	1.818	0.1818
9	1.939	0.0613
10	1.980	0.01980
11	1.998	0.001988

Table 2: Function used for the gradation-Quadratic Function:

$$E(x) = (3E_2 + 3E_1 - 6)x^2 + (-2E_2 - 4E_1 + 6)x + E_1$$

Microstructure	E_1 (MPa)	E_2 (MPa)
1	0.001	1
2	0.001	0.1
3	0.01	0.3162
4	0.1	1
5	0.6	1.897
6	1	1
7	0.2217	0.0701
8	0.4151	0.04151
9	0.7411	0.02344
10	1.684	0.01684
11	1.9	0.0019

Table 3: Function used for the gradation-Exponential Function:

$$E(x) = E_1 exp[ln(\frac{E_2}{E_1})x]$$

Microstructure	E_1 (MPa)	E_2 (MPa)
1	0.006915	6.915
2	0.04652	4.652
3	0.1128	3.567
4	0.2558	2.558
5	0.5324	1.684
6	1	1
7	1.684	0.5324
8	2.558	0.2558
9	3.567	0.1128
10	4.652	0.04652
11	6.915	0.006915

Table 4: Function used for the gradation-Cosine Function:

$$E(x) = E_0[1 + \frac{\rho-1}{\rho+1}cos(2\pi x)]$$

Microstructure	E_0 (MPa)	ρ
1	1	1
2	1	2
3	1	3
4	1	4
5	1	5
6	1	6

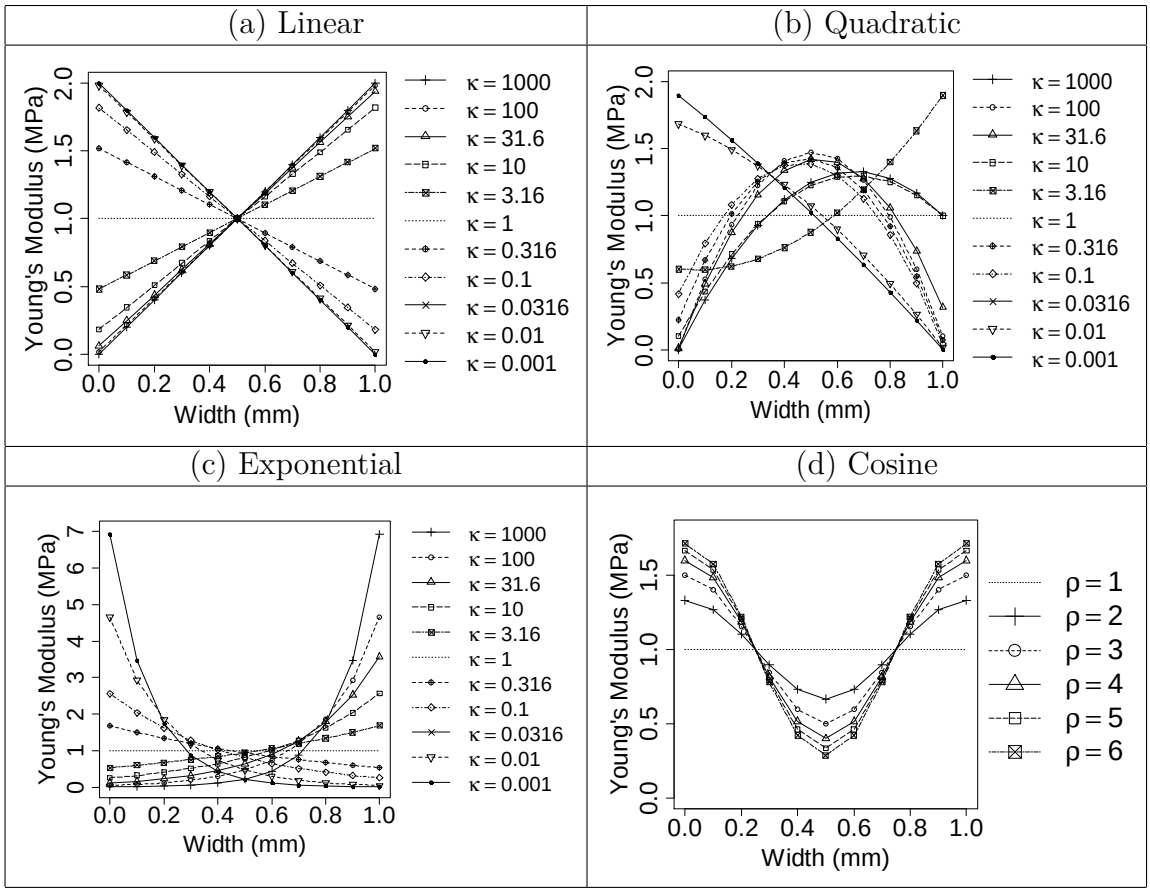

Figure 3: Plots of Material Contrast (κ and ρ) as a function of (Width, Young's Modulus)

Chapter 4

Results and Discussion

We begin by first validating our Finite Element model with selected benchmark problems published in the literature. Next, the fracture response of Functionally Graded Materials (FGMs) under membrane loading is analyzed as a function of material contrast and crack length. Subsequently, the notion of 'design maps' is introduced using which admissible regions for the design of microstructures with enhanced fracture resistance can be obtained[1].

4.1 Model Validation

The validation of Finite Element (FE) results is a very necessary step before proceeding to construct the 'design maps'. For this purpose, FE models were developed for homogeneous and FGM strips subjected to membrane loading (see Fig. 4). The FE model for each specimen was then calibrated by comparing the predicted results with the ones published in the literature.

4.1.1. Stress Intensity Factors For Homogeneous Materials. A numerical model was setup in order to extract the Stress Intensity Factors for a homogeneous strip with an edge crack as seen in Fig. (4). Here, W is the width of the strip, L is the length of the strip, σ is the stress applied and a is the crack length. Following Rao and Rahman [16], the variables were set as follows: $\sigma = 1$ MPa, W = 1 mm, L = 4 mm. In addition, a range of crack lengths between 0.2 mm and 0.6 mm were investigated (a = 0.2, 0.3, 0.4, 0.5 and 0.6 mm). The boundary conditions used for FE modeling are shown in Fig. (4) in which point A was pinned and the edge BA was restricted from movement in the vertical direction. Half the geometry

[1]See also [53] M. R. Murshed, S. I. Ranganathan, and F. H. Abed, "Design maps for fracture resistant functionally graded materials," *European Journal of Mechanics - A/Solids*, vol. 58, pp. 31 – 41, 2016. [Online]. Available: http://www.sciencedirect.com/science/article/pii/S0997753816000036

was numerically simulated by using symmetry boundary conditions and Barsoum elements were used at the crack tip [54, 55]. The material was assumed elastic with $E = 2$ MPa, $v = 0.3$ and a plane strain condition was specified.

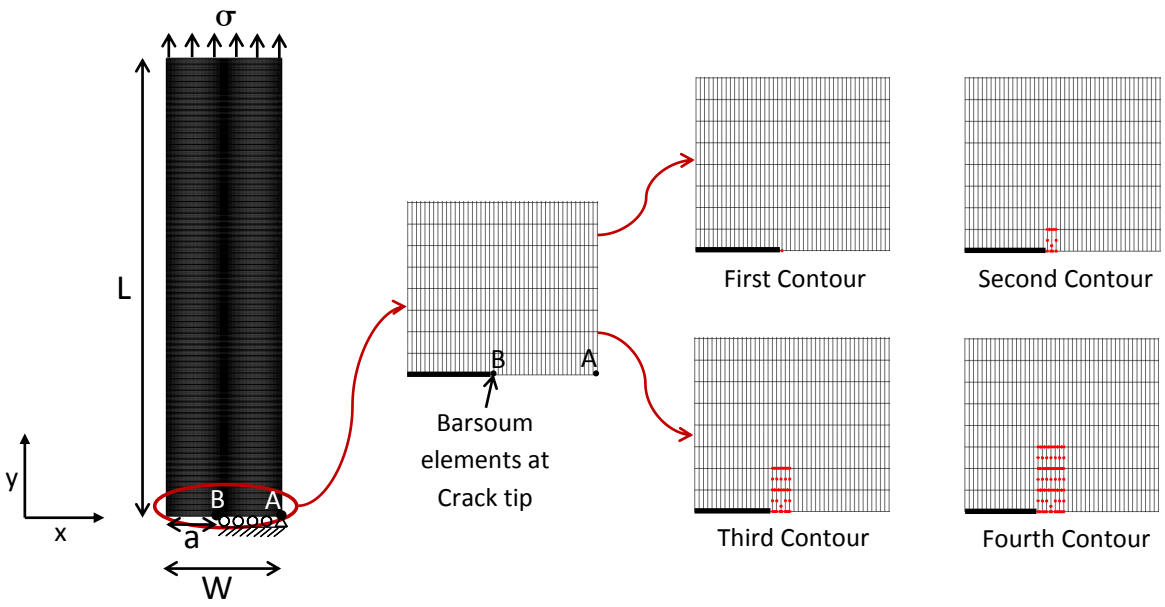

Figure 4: Homogeneous/FGM Strip with various contours for evaluating the J-integral

Next, model verification was conducted and a comparison was made with Chen et al. [56] in terms of the normalized Stress Intensity Factor defined as follows

$$K_0 = \frac{K_I}{\sigma\sqrt{\pi a}} \tag{18}$$

where, σ is the applied stress, a is the crack length and K_I is the Stress Intensity Factor. The results obtained for normalized Stress Intensity Factors, K_0 are benchmarked with the analytical results obtained by Chen et al. [56] as presented in TABLE (5). It is evident from TABLE (5) that the present FE model is capable of predicting accurate results as the percentage difference is less than 1% for all crack lengths.

Table 5: Model Verification of a homogeneous strip for various Crack Lengths (a)

a (mm)	Current Work	Chen et al. [56]	% difference with [56]
0.2	1.3633	1.3734	0.7
0.3	1.6554	1.6627	0.4
0.4	2.1055	2.1065	0.05
0.5	2.8158	2.8297	0.5
0.6	4.018	4.0301	0.3

4.1.2. Stress Intensity Factors For Functionally Graded Materials. We will now discuss the exponential variation of the Young's Modulus which was employed using Eq. (16) on the FGM Strip (see Fig. 4). The benchmark cases that were taken into consideration include Finite Element Analysis carried out by Rao and Rahman [16], Erdogan and Wu [13], Chen et al. [56] and Kim and Paulino [18]. In order to quantify the material contrast, the following variable κ is defined as

$$\kappa = \frac{E_2}{E_1} \tag{19}$$

In the present analysis, four material contrasts of $\kappa = 0.1$, 0.2, 5 and 10 were examined. The predicted results for normalized Stress Intensity Factors were compared with four different studies as listed in TABLES (6-9). A range of crack lengths between 0.2 mm and 0.6 mm were investigated ($a = 0.2$, 0.3, 0.4, 0.5 and 0.6 mm). Comparison of the results obtained with reference solutions reinforced the validity of the FE models. For example, computational results showed that the percentage difference with respect to Rao and Rahman [16] is less than 6% for $\kappa = 0.1$, less than 5% for $\kappa = 0.2$, less than 3% for $\kappa = 5$ and less than 5% for $\kappa = 10$. In addition, the plots for the above TABLES can be seen in Fig. (5). It can be observed that normalized SIF increases with an increase in crack lengths for all material contrasts. Similar trends were observed by various authors such as Jin and Paulino [57] and Noda and Lan [58].

In the next section, the validated FE model in Fig. (4) will be utilized to analyze the fracture response of Functionally Graded Materials as a function of material contrast and crack length. Several functional distributions will be considered in order to construct 'design maps' which unify the treatment of heterogeneous microstructures.

Table 6: Model verification for different Crack Lengths (a) with $\kappa = 0.1$

a (mm)	Current Work	Rao & Rahman [16]	Erdogan & Wu [13]	Chen et al. [56]	Kim & Paulino [18]	% difference with [16]
0.2	1.2659	1.3374	1.2965	1.3193	1.284	5.3
0.3	1.7889	1.8976	1.8581	1.8642	1.846	5.7
0.4	2.4552	2.5938	2.5699	2.5588	2.544	5.3
0.5	3.381	3.5472	3.5701	3.5213	3.496	4.7
0.6	4.8069	4.9956	5.188	5.0726	4.962	3.8

Table 7: Model verification for different Crack Lengths (a) with $\kappa = 0.2$

a (mm)	Current Work	Rao & Rahman [16]	Erdogan & Wu [13]	Chen et al. [56]	Kim & Paulino [18]	% difference with [16]
0.2	1.3766	1.4193	1.3956	1.4188	1.39	3.0
0.3	1.7843	1.8668	1.8395	1.8497	1.831	4.4
0.4	2.3688	2.4657	2.4436	2.4486	2.431	3.9
0.5	3.2134	3.3297	3.3266	3.3234	3.292	3.5
0.6	4.5609	4.6905	4.7614	4.786	4.669	2.8

Table 8: Model verification for different Crack Lengths (a) with $\kappa = 5$

a (mm)	Current Work	Rao & Rahman [16]	Erdogan & Wu [13]	Chen et al. [56]	Kim & Paulino [18]	% difference with [16]
0.2	1.1592	1.1269	1.1318	1.1622	1.132	2.9
0.3	1.4011	1.3754	1.3697	1.3899	1.37	1.9
0.4	1.7867	1.7576	1.7483	1.7746	1.749	1.7
0.5	2.4146	2.3772	2.3656	2.4125	2.366	1.6
0.6	3.5083	3.4478	3.4454	3.5736	3.448	1.8

Table 9: Model verification for different Crack Lengths (a) with $\kappa = 10$

a (mm)	Current Work	Rao & Rahman [16]	Erdogan & Wu [13]	Chen et al. [56]	Kim & Paulino [18]	% difference with [16]
0.2	1.0388	0.9958	1.0019	1.0324	1.003	4.3
0.3	1.2719	1.2343	1.2291	1.2499	1.228	3.0
0.4	1.6419	1.598	1.5884	1.6146	1.588	2.7
0.5	2.2467	2.1889	2.1762	2.2234	2.175	2.6
0.6	3.3065	3.2167	3.2124	3.3371	3.212	2.8

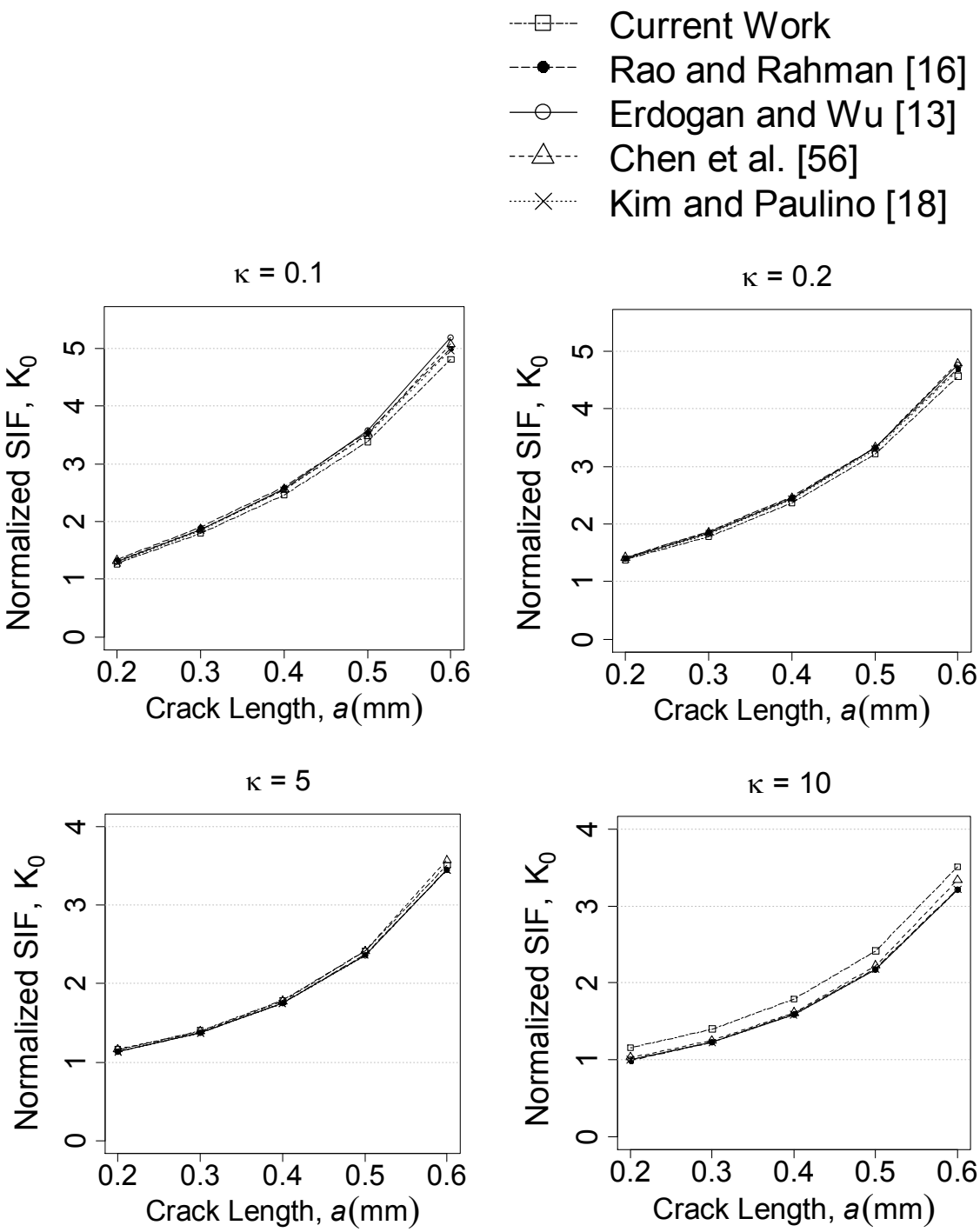

Figure 5: Model verification for varying material contrasts, κ

4.2 Functionally Graded Materials Under Membrane Loading

We now consider the fracture response of several Functionally Graded Materials (FGMs) as a function of the non-dimensional crack length, $\frac{a}{W}$ and material contrasts (κ and ρ)[2]. At this stage, it is convenient to introduce the Fracture Index (ϕ) as follows [53]

$$\phi = \frac{K_0^{FGM}}{K_0^{hom}} \tag{20}$$

where K_0^{FGM} and K_0^{hom} are the normalized Stress Intensity Factors for a Functionally Graded Material and its equivalent homogeneous material, respectively. When $\phi < 1$, the fracture resistance of FGM is better than the homogeneous material and vice-versa.

Fig. (6a) shows that for linear functions with contrasts greater than 1, the FGM is superior to its homogeneous counterpart since $\phi < 1$. It can also be noted that for smaller crack lengths ($\frac{a}{W} \leq 0.3$), FGM is always advantageous over a homogeneous material irrespective of the material contrast. This is not the case for larger non-dimensional crack lengths. Similarly, Fig. (6b) demonstrates that quadratic functions with all material contrasts and $\frac{a}{W}$ ranging from 0.2 to 0.3 can be employed for designing fracture resistant microstructures. Also, when $\frac{a}{W} = 0.4$ and $\kappa \geq 1$, FGM outperforms the homogeneous material and vice-versa. For $\frac{a}{W} > 0.4$, the use of quadratic functional gradation is not beneficial for any contrast κ. Likewise, Fig. (6c) illustrates that exponential gradation with contrasts greater than 1 is always beneficial irrespective of $\frac{a}{W}$. Along similar lines, Fig. (6d) shows that cosine functions with $\frac{a}{W} \leq 0.4$ have enhanced fracture resistance irrespective of the material contrast, ρ. In the next section, 'design maps' highlighting the admissible regions for constructing fracture resistant microstructures will be illustrated.

[2]See also [59] M. R. Murshed, S. I. Ranganathan, and F. H. Abed, "Effect of material contrast and crack length on the fracture of functionally graded materials," *Mach Conference*, Annapolis, MD, USA, 2015.

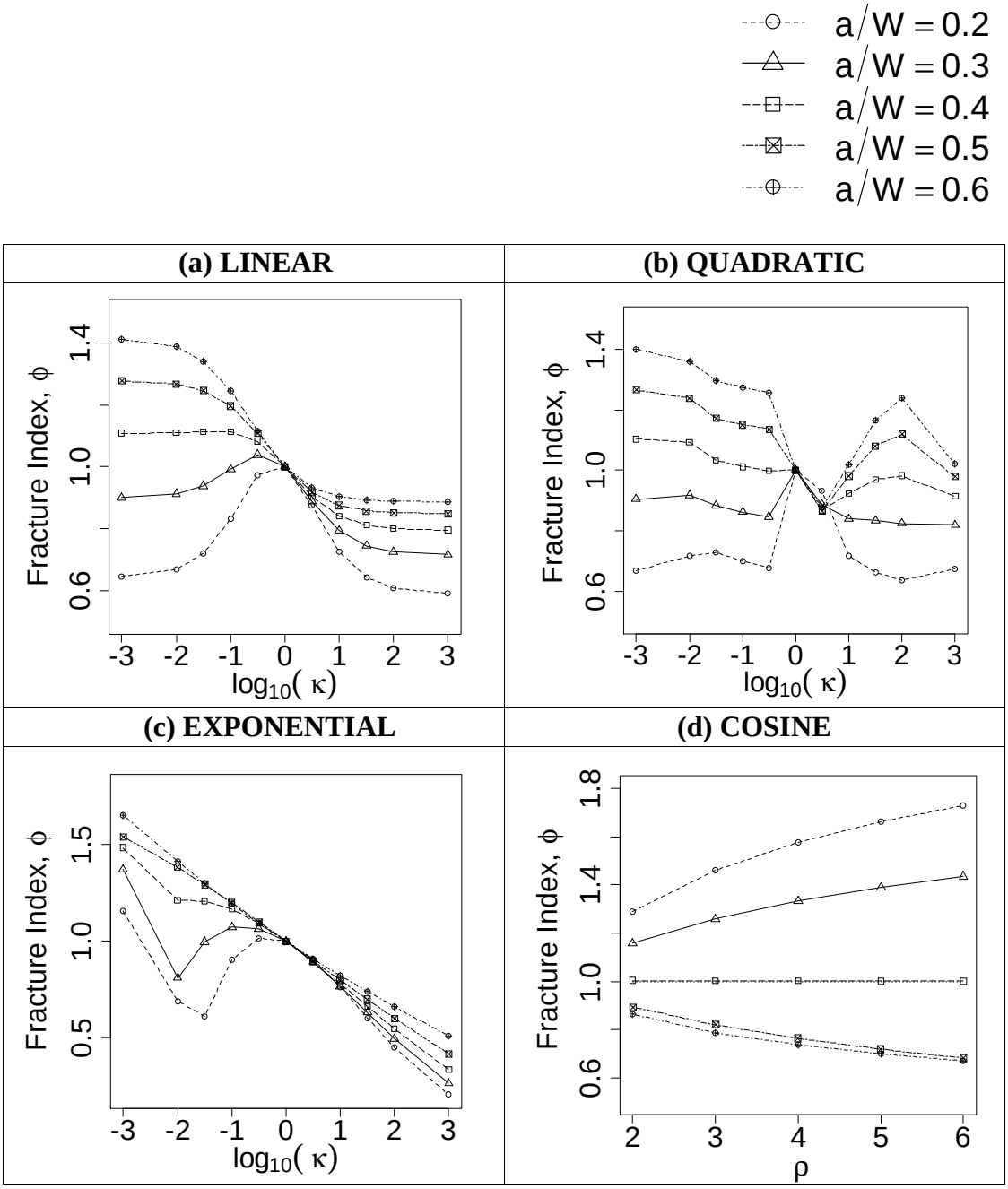

Figure 6: Plots of non-dimensional Crack Length ($\frac{a}{W}$) as functions of ($\log_{10}(\kappa)$, ϕ) and (ρ,ϕ)

4.3 Design Maps

With the framework laid out in the previous section, it is now possible to construct 'design maps' to unify the treatment of FGMs. Such maps can be visualized as contours of Fracture Index, ϕ in the $(\frac{a}{W}\ ,\ log_{10}(\kappa))$ space (see Fig. 7). As discussed before, regions with $\phi < 1$ highlight microstructures with enhanced fracture resistance. From Fig. (7a), it is evident that as long as $\kappa > 1$, FGMs with linear gradation in the modulus have enhanced fracture resistance irrespective of the crack length. This is also the case when $\frac{a}{W} < 0.4$ irrespective of the material contrast. Similarly, a quadratic functional gradation [see Fig. (7b)] is beneficial when $\frac{a}{W} < 0.4$ (irrespective of material contrast). The 'Fracture Index' is greater than one for all other combinations of $\frac{a}{W}$, $log_{10}(\kappa)$. Hence, such quadratric FGMs result in designs which are inferior to the homogeneous materials. Finally, exponential functions offer enhanced fracture resistance when $\kappa > 1$ (see Fig. 7c).

Alternatively, the 'design maps' can be visualized as contours of Fracture Index, ϕ in the $(\frac{a}{W}\ ,\ \frac{dE}{dx})$ space (see Fig. 8). Here, $(\frac{dE}{dx})$ is the local gradient of Young's Modulus evaluated at the crack tip. Although $(\frac{dE}{dx})$ is a dependent variable, it offers a different perspective into the design of fracture resistant microstructures. As mentioned before, regions with $\phi < 1$ highlight microstructures with enhanced fracture resistance. From Fig. (8a), it can be seen that for FGMs with linear variation in the Young's Modulus, almost any $\frac{dE}{dx}$ (negative or positive) is beneficial irrespective of the crack length. Likewise, a quadratic functional distribution [see Fig. (8b)] offer enhanced fracture resistance when $\frac{a}{W} < 0.4$ for all combinations of $\frac{dE}{dx}$ (negative or positive). Lastly, exponential functions with $\frac{dE}{dx} < 0$ will result in FGMs that are superior to homogeneous materials as the 'Fracture Index' is less than one for all crack lengths (see Fig. 8c).

(a) LINEAR

(b) QUADRATIC

(c) EXPONENTIAL

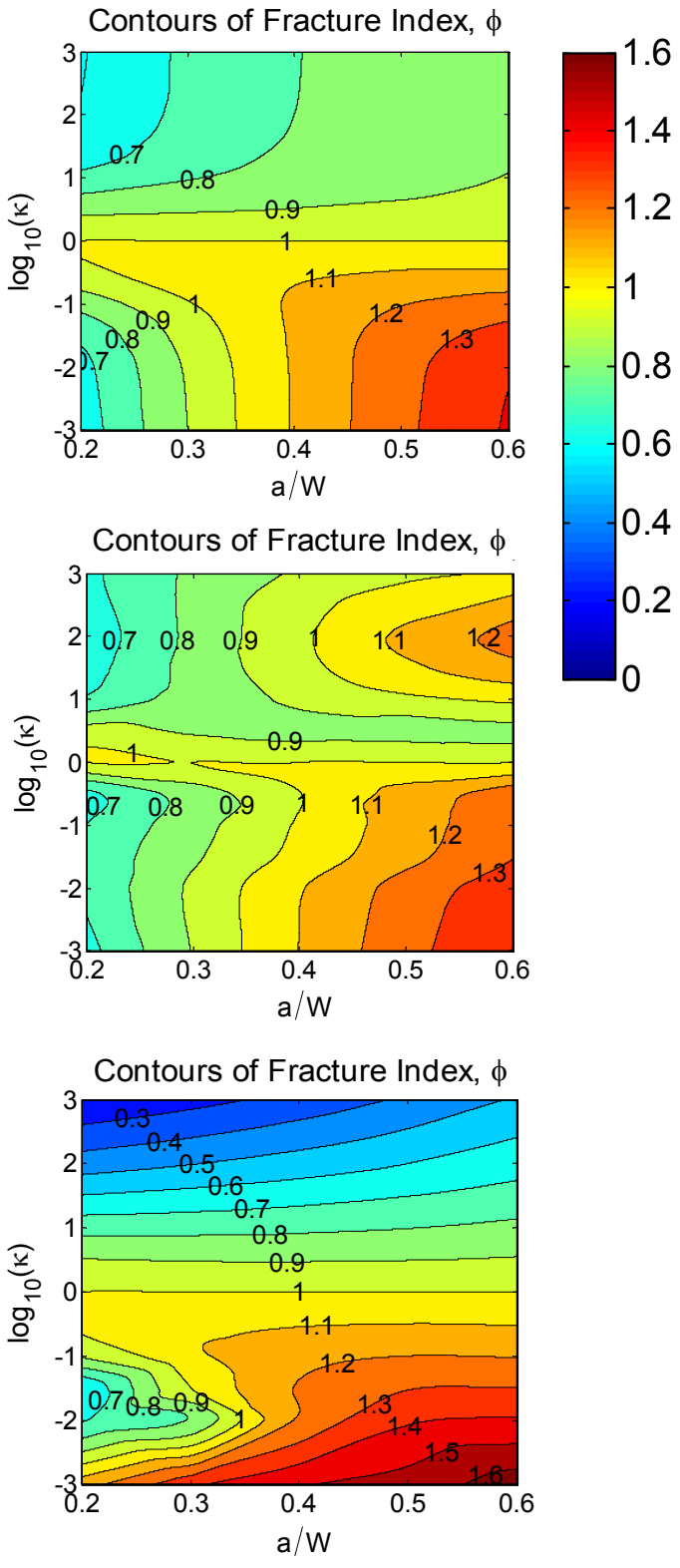

Figure 7: Contour Plots of Fracture Index (ϕ) as a function of Material Contrast (κ) and non-dimensional Crack Length ($\frac{a}{W}$)

(a) LINEAR

(b) QUADRATIC

(c) EXPONENTIAL

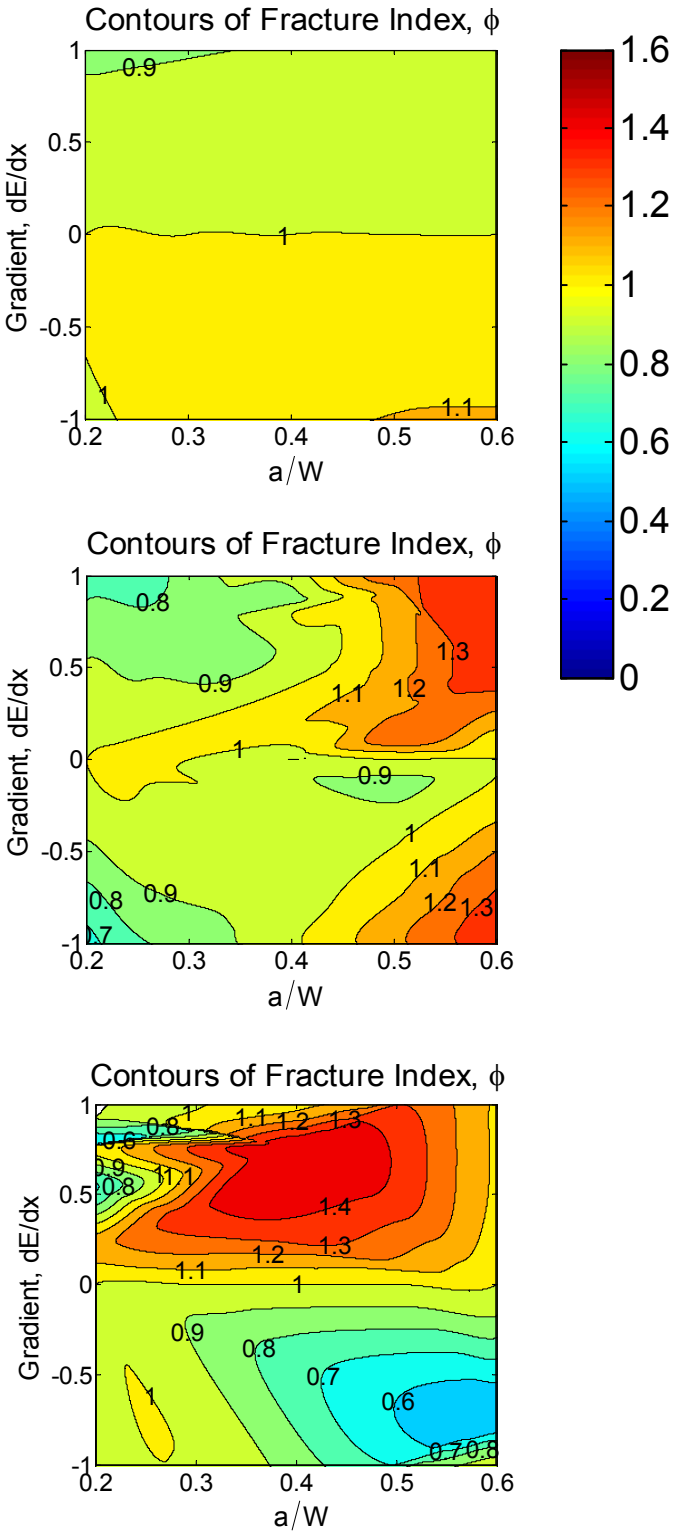

Figure 8: Contour Plots of Fracture Index (ϕ) as a function of Elastic Gradient at Crack Tip ($\frac{dE}{dx}$) and non-dimensional Crack Length ($\frac{a}{W}$)

These observations are also summarized in Fig. (9a, b & c), where arrows indicate appropriate quadrants in the 'design maps' with enhanced fracture resistance.

(a) LINEAR

(b) QUADRATIC

(c) EXPONENTIAL

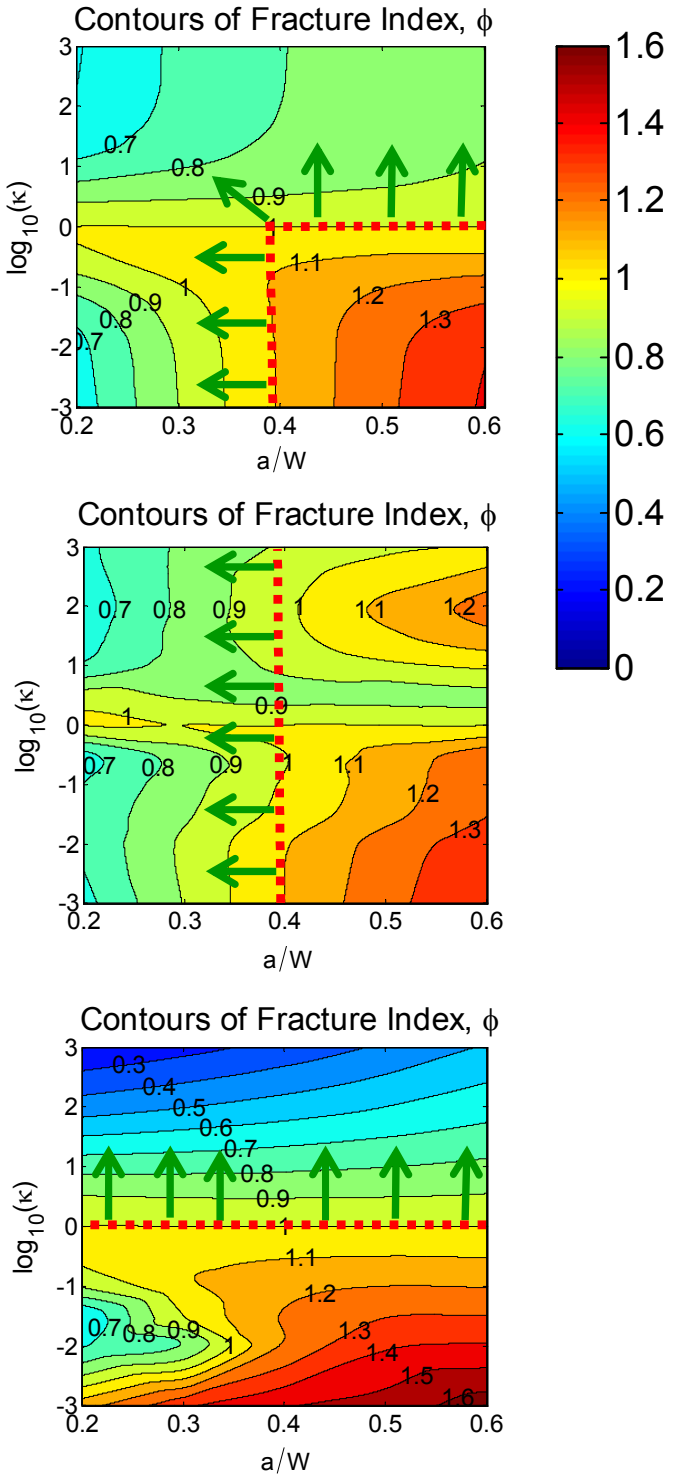

Figure 9: Admissible Regions in the Design Space illustrated by green arrows

We now discuss the analytical relationship between κ, $\frac{a}{W}$ and ϕ in a certain asymptotic limit for exponential functions as follows

$$\phi \approx 1 + mlog_{10}(\kappa), \qquad \frac{a}{W} > 0.4 \tag{21}$$

where, m = -0.194 and m = -0.1636 for $\frac{a}{W} = 0.5$ and $\frac{a}{W} = 0.6$, respectively. The material contrast, κ can be used to determine the Fracture Index, ϕ values for crack lengths greater than 0.4 as shown in TABLE (10).

Table 10: Fracture Index, ϕ values for varying material contrasts, κ

κ	ϕ for $\frac{a}{W} = 0.5$	ϕ for $\frac{a}{W} = 0.6$
1	1	1
10	0.80	0.83
100	0.61	0.67
1000	0.42	0.51

The values of Fracture Index, ϕ from TABLE (10) are superimposed on the design map for exponential gradation (see Fig. 10) for $\frac{a}{W} = 0.5$ and $\frac{a}{W} = 0.6$. Hence, the analytical relationship in Eq. (21) can be employed to predict the Fracture Index values for $\kappa \geq 1$.

It is now important to highlight that the 'Fracture Index' values from the model validation studies conducted can also be visualized as points on the design map for exponential gradation (see Fig. 11). These results validate data points published in the literature by various authors such as Rao and Rahman [16], Erdogan and Wu [13], Chen et al. [56] and Kim and Paulino [18]. In addition, experimental data can be superimposed on the design map which highlights the universality of such maps as any Functionally Graded Material can be mapped as a point on the $(a - \kappa)$ space.

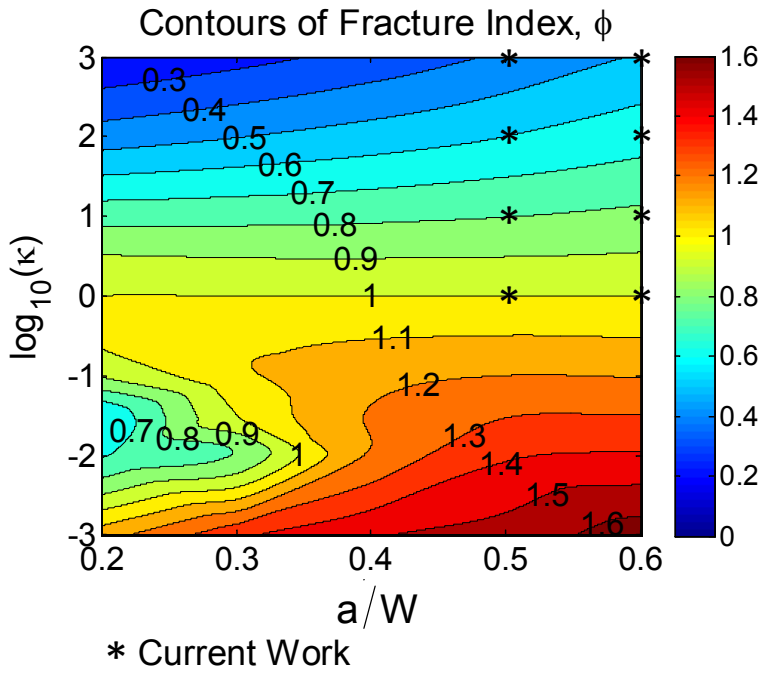

Figure 10: Design Map highlighting the Fracture Index (ϕ) values at $\frac{a}{W} = 0.5$ and $\frac{a}{W} = 0.6$

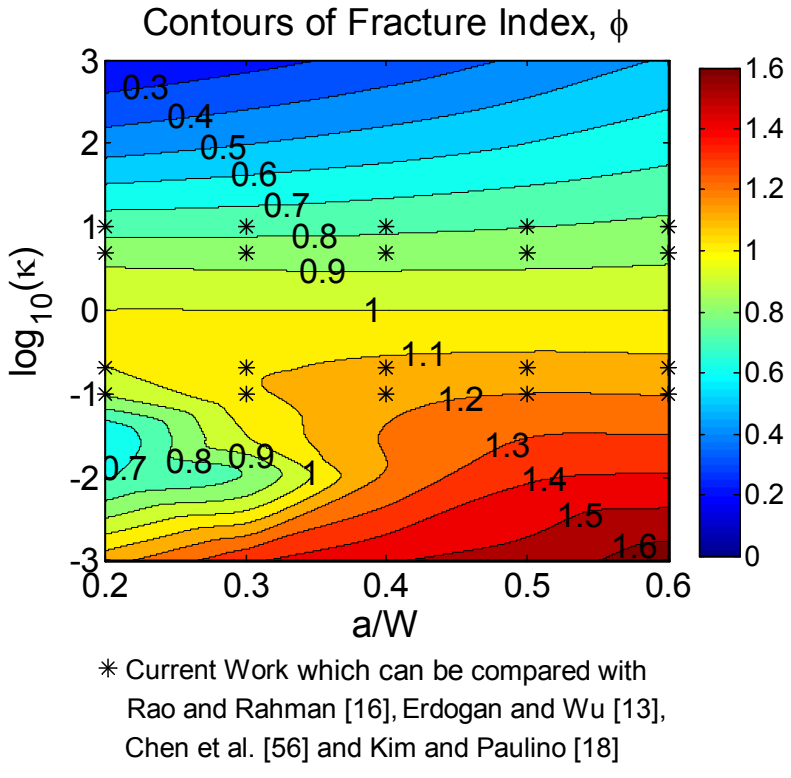

Figure 11: Design Map highlighting the Fracture Index (ϕ) values for exponential gradation (Current Work)

In summary, the following observations can be inferred from the 'design maps' (see Fig. 12): i) In region (a), FGMs with all distributions (linear, quadratic & exponential) offer enhanced fracture resistance; ii) In region (b), the use of exponential distribution is not beneficial; iii) In region (c), only the use of linear and exponential distributions offer enhancement in fracture resistance; iv) In region (d), the use of FGMs is not recommended since the 'Fracture Index' is always greater than one irrespective of the functional distribution; v) When the crack size is small, the 'Fracture Index' values are almost the same irrespective of the specific functional distribution or the material contrast used; vi) Again, when κ is close to one, the 'Fracture Index' virtually remains the same irrespective of the functional distribution used or the specific value of $\frac{a}{W}$; vii) When $\kappa = 1$, the 'Fracture Index' $\phi = 1$ and this is a horizontal line in the design map representing a homogeneous material.

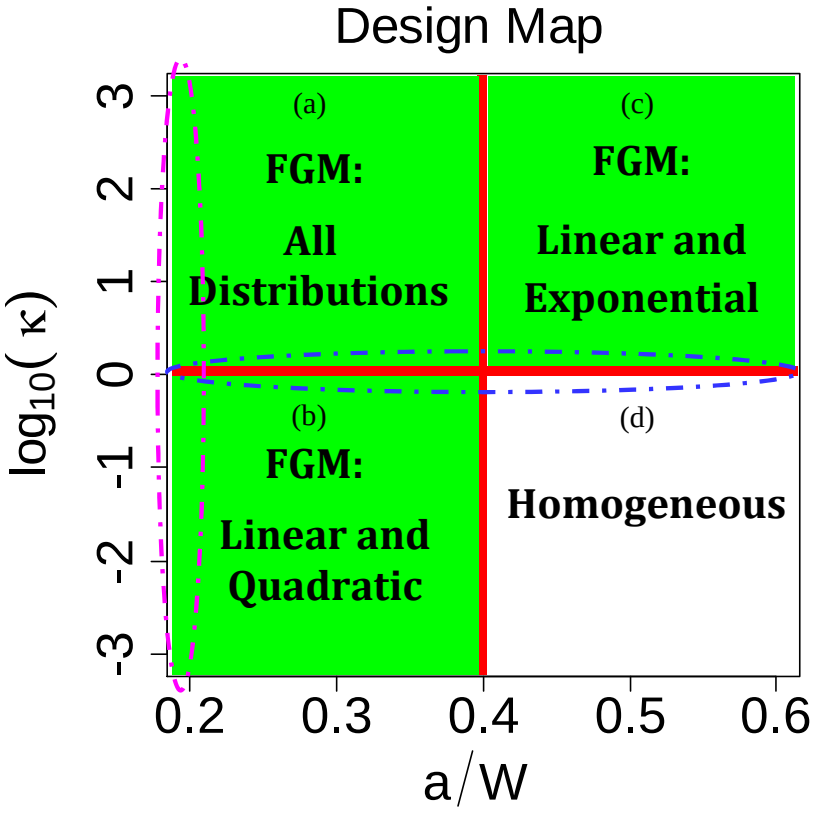

Figure 12: Design Map for Fracture Resistant Materials

Chapter 5

Conclusion and Future Work

In this thesis, several spatial variations for the Young's Modulus were used to generate 'design maps' highlighting the admissible regions for the design of microstructures with enhanced fracture resistance. In chapter 2, we demonstrated the mathematical background for obtaining the J-integral and its relation to the Stress Intensity Factor for a linear elastic material under mode-I loading. In chapter 3, we presented the methodology employed in this research. It has to be noted that in order to objectively compare various functional gradations, all microstructures considered in this study have the same volume averaged Young's Modulus. Based on this constraint, several functionally graded microstructures were created and the functions examined were linear, quadratic, exponential and cosine.

In chapter 4, several Functionally Graded Materials (FGMs) with an edge crack length (a) and membrane loading were considered and the resulting J-integral values were obtained numerically using Finite Element Analysis. The averages of the J-integral values were used to determine the normalized Stress Intensity Factors which were then benchmarked with existing analytical solutions in special cases. This approach was repeated for a variety of material contrasts (κ) and crack lengths. Subsequently, the concept of 'Fracture Index' was also introduced and its relevance to compare a FGM to a homogeneous material was presented. It was demonstrated that Functionally Graded Materials can be superior or inferior to the reference homogeneous material depending upon the crack length, type of gradation and material contrast.

On a final note, the concepts illustrated in this thesis can be applied to mode-II, mode-III and mixed mode fracture problems in order to construct 'design maps' that demonstrate admissible regions where the fracture toughness of FGMs is maximized.

Although, only select functional distributions have been evaluated in this research, other FGMs (for instance a Taylor's Series expansion of the Modulus with higher order terms included) can be easily studied and the results can be projected on the 'design maps', thereby highlighting the universality of such maps. Finally, the 'design maps' offer a simple, yet powerful framework to enable the rational design of fracture resistant Functionally Graded Materials.

References

[1] Z. Luo, X. Zhou, and J. Yu, "High-temperature mechanical properties of thermal barrier coated SiC/SiC composites by PIP process with a new precursor polymer," *Surface and Coatings Technology*, vol. 258, pp. 146–153, 2014.

[2] W. Krenkel and F. Berndt, "C/C–SiC composites for space applications and advanced friction systems," *Materials Science and Engineering: A*, vol. 412, no. 1–2, pp. 177 – 181, 2005.

[3] S. I. Ranganathan, F. H. Abed, and M. G. Aldadah, "Buckling of slender columns with functionally graded microstructures," *Mechanics of Advanced Materials and Structures*, vol. 23, no. 11, pp. 1360–1367, 2016.

[4] M. Aldadah, S. I. Ranganathan, and F. H. Abed, "Buckling of two phase inhomogeneous columns at arbitrary phase contrasts and volume fractions," *Journal of Mechanics of Materials and Structures*, vol. 9, no. 5, pp. 465–474, 2014.

[5] M. Bodaghi, A. Damanpack, M. Aghdam, and M. Shakeri, "Geometrically non-linear transient thermo-elastic response of FG beams integrated with a pair of FG piezoelectric sensors," *Composite Structures*, vol. 107, pp. 48–59, 2014.

[6] M. Gasik and Y. Bilotsky, "Optimisation of functionally gradated material thermoelectric cooler for the solar space power system," *Applied Thermal Engineering*, vol. 66, no. 1, pp. 528–533, 2014.

[7] M. Mehrali, F. S. Shirazi, M. Mehrali, H. S. C. Metselaar, N. A. B. Kadri, and N. A. A. Osman, "Dental implants from functionally graded materials," *Journal of Biomedical Materials Research Part A*, vol. 101, no. 10, pp. 3046–3057, 2013.

[8] F. Watari, A. Yokoyama, M. Omori, T. Hirai, H. Kondo, M. Uo, and T. Kawasaki, "Biocompatibility of materials and development to functionally graded implant for bio-medical application," *Composites Science and Technology*, vol. 64, no. 6, pp. 893 – 908, 2004.

[9] S. L. Sing, J. An, W. Y. Yeong, and F. E. Wiria, "Laser and electron-beam powder-bed additive manufacturing of metallic implants: A review on processes, materials and designs," *Journal of Orthopaedic Research*, vol. 34, no. 3, pp. 369–385, 2016.

[10] P. Bartolo, J.-P. Kruth, J. Silva, G. Levy, A. Malshe, K. Rajurkar, M. Mitsuishi, J. Ciurana, and M. Leu, "Biomedical production of implants by additive electro-chemical and physical processes," *CIRP Annals-Manufacturing Technology*, vol. 61, no. 2, pp. 635–655, 2012.

[11] R. Gibson, "Some results concerning displacements and stresses in a non-homogeneous elastic half-space," *Geotechnique*, vol. 17, no. 1, pp. 58–67, 1967.

[12] F. Delale and F. Erdogan, "The crack problem for a nonhomogeneous plane," *Journal of Applied Mechanics*, vol. 50, no. 3, pp. 609–614, 1983.

[13] F. Erdogan and B. Wu, "The surface crack problem for a plate with functionally graded properties," *Journal of Applied Mechanics*, vol. 64, no. 3, pp. 449–456, 1997.

[14] Y. Chan, G. Paulino, and A. Fannjiang, "The crack problem for nonhomogeneous materials under antiplane shear loading — a displacement based formulation," *International Journal of Solids and Structures*, vol. 38, no. 17, pp. 2989 – 3005, 2001.

[15] J. Dolbow and M. Gosz, "On the computation of mixed-mode stress intensity factors in functionally graded materials," *International Journal of Solids and Structures*, vol. 39, no. 9, pp. 2557 – 2574, 2002.

[16] B. Rao and S. Rahman, "Mesh-free analysis of cracks in isotropic functionally graded materials," *Engineering Fracture Mechanics*, vol. 70, no. 1, pp. 1 – 27, 2003.

[17] J. W. Eischen, "Fracture of nonhomogeneous materials," *International Journal of Fracture*, vol. 34, no. 1, pp. 3–22, 1987.

[18] J.-H. Kim and G. H. Paulino, "Finite element evaluation of mixed mode stress intensity factors in functionally graded materials," *International Journal for Numerical Methods in Engineering*, vol. 53, no. 8, pp. 1903–1935, 2002.

[19] P. Gu, M. Dao, and R. Asaro, "A simplified method for calculating the crack-tip field of functionally graded materials using the domain integral," *Journal of Applied Mechanics*, vol. 66, no. 1, pp. 101–108, 1999.

[20] P. Gu and R. Asaro, "Cracks in functionally graded materials," *International Journal of Solids and Structures*, vol. 34, no. 1, pp. 1–17, 1997.

[21] G. Bao and L. Wang, "Multiple cracking in functionally graded ceramic/metal coatings," *International Journal of Solids and Structures*, vol. 32, no. 19, pp. 2853–2871, 1995.

[22] G. Bao and H. Cai, "Delamination cracking in functionally graded coating/metal substrate systems," *Acta Materialia*, vol. 45, no. 3, pp. 1055–1066, 1997.

[23] G. Anlas, M. Santare, and J. Lambros, "Numerical calculation of stress intensity factors in functionally graded materials," *International Journal of Fracture*, vol. 104, no. 2, pp. 131–143, 2000.

[24] M. Hossain, C.-J. Hsueh, B. Bourdin, and K. Bhattacharya, "Effective toughness of heterogeneous media," *Journal of the Mechanics and Physics of Solids*, vol. 71, pp. 15–32, 2014.

[25] A. A. Abd-Elhady and H. E.-D. M. Sallam, "Crack sensitivity of bolted metallic and polymeric joints," *Engineering Fracture Mechanics*, vol. 147, pp. 55–71, 2015.

[26] M. Aliha, G. R. Hosseinpour, and M. Ayatollahi, "Application of cracked triangular specimen subjected to three-point bending for investigating fracture behavior of rock materials," *Rock Mechanics and Rock Engineering*, vol. 46, no. 5, pp. 1023–1034, 2013.

[27] S. Dancette, D. Fabregue, R. Estevez, V. Massardier, T. Dupuy, and M. Bouzekri, "A finite element model for the prediction of advanced high strength steel spot welds fracture," *Engineering Fracture Mechanics*, vol. 87, pp. 48–61, 2012.

[28] J. R. Rice, "A path independent integral and the approximate analysis of strain concentration by notches and cracks," *Journal of Applied Mechanics*, vol. 35, no. 2, pp. 379–386, 1968.

[29] F. Erdogan, "Stress intensity factors," *Journal of Applied Mechanics*, vol. 50, no. 4b, pp. 992–1002, 1983.

[30] M. Williams, "On the stress distribution at the base of a stationary crack," *Journal of Applied Mechanics*, vol. 24, pp. 109–114, 1957.

[31] T. Honein and G. Herrmann, "Conservation laws in nonhomogeneous plane elastostatics," *Journal of the Mechanics and Physics of Solids*, vol. 45, no. 5, pp. 789–805, 1997.

[32] C. Shih, B. Moran, and T. Nakamura, "Energy release rate along a three-dimensional crack front in a thermally stressed body," *International Journal of Fracture*, vol. 30, no. 2, pp. 79–102, 1986.

[33] Abaqus Theory Manual, "J-Integral evaluation," *Dassault Systemes*, Providence, Rhode Island, USA, 2012.

[34] M. Nikbakht and N. Choupani, "Numerical investigation of delamination in carbon-epoxy composite using arcan specimen," *International Journal of Mechanical, Industrial and Aerospace Engineering*, vol. 2, no. 4, pp. 259–266, 2008.

[35] E. Martínez-Pañeda and R. Gallego, "Numerical analysis of quasi-static fracture in functionally graded materials," *International Journal of Mechanics and Materials in Design*, pp. 1–20, 2014.

[36] Abaqus Theory Manual, "Stress Intensity Factor extraction," *Dassault Systemes*, Providence, Rhode Island, USA, 2012.

[37] C. Shih and R. Asaro, "Elastic-plastic analysis of cracks on bimaterial interfaces: part I—small scale yielding," *Journal of Applied Mechanics*, vol. 55, no. 2, pp. 299–316, 1988.

[38] D. Barnett and R. Asaro, "The fracture mechanics of slit-like cracks in anisotropic elastic media," *Journal of the Mechanics and Physics of Solids*, vol. 20, no. 6, pp. 353–366, 1972.

[39] F. Fischer, N. Simha, J. Predan, R. Schöngrundner, and O. Kolednik, "On configurational forces at boundaries in fracture mechanics," *International Journal of Fracture*, vol. 174, no. 1, pp. 61–74, 2012.

[40] M. Bernard, J. W. Provan, and H. Lakshiminarayana, "On the development of a fracture toughness test procedure using a notched disk specimen," *ASTM Special Technical Publication*, vol. 1204, pp. 143–161, 1993.

[41] Abaqus Analysis User's Manual, "Contour Integral evaluation," *Dassault Systemes*, Providence, Rhode Island, USA, 2012.

[42] W. Brocks and I. Scheider, "Numerical aspects of the path-dependence of the J-Integral in incremental plasticity," *GKSS Forschungszentrum, Geesthacht, Germany, Technical Report No. GKSS/WMS/01/08 (2001)*, 2001.

[43] M. Kamaya, "J-Integral solutions for surface crack inside pipe under bending load," *Journal of Solid Mechanics and Materials Engineering*, vol. 3, no. 10, pp. 1115–1126, 2009.

[44] Y.-J. Kim, J.-S. Kim, Y.-Z. Lee, and Y.-J. Kim, "Non-linear fracture mechanics analyses of part circumferential surface cracked pipes," *International Journal of Fracture*, vol. 116, no. 4, pp. 347–375, 2002.

[45] C. Bayley and R. Bell, "Parametric investigation into the coalescence of coplanar fatigue cracks," *International Journal of Fatigue*, vol. 21, no. 4, pp. 355–360, 1999.

[46] J.-H. Kim and G. H. Paulino, "An accurate scheme for mixed-mode fracture analysis of functionally graded materials using the interaction integral and micromechanics models," *International Journal for Numerical Methods in Engineering*, vol. 58, no. 10, pp. 1457–1497, 2003.

[47] Z.-H. Jin and R. Batra, "Some basic fracture mechanics concepts in functionally graded materials," *Journal of the Mechanics and Physics of Solids*, vol. 44, no. 8, pp. 1221–1235, 1996.

[48] J. Yau, S. Wang, and H. Corten, "A mixed-mode crack analysis of isotropic solids using conservation laws of elasticity," *Journal of Applied Mechanics*, vol. 47, no. 2, pp. 335–341, 1980.

[49] Z. Zhong and Z. Cheng, "Fracture analysis of a functionally graded strip with arbitrary distributed material properties," *International Journal of Solids and Structures*, vol. 45, no. 13, pp. 3711–3725, 2008.

[50] I. Elishakoff and Z. Guede, "Analytical polynomial solutions for vibrating axially graded beams," *Mechanics of Advanced Materials and Structures*, vol. 11, no. 6, pp. 517–533, 2004.

[51] L.-C. Guo and N. Noda, "Modeling method for a crack problem of functionally graded materials with arbitrary properties—piecewise-exponential model," *International Journal of Solids and Structures*, vol. 44, no. 21, pp. 6768 – 6790, 2007.

[52] P. Fratzl, H. S. Gupta, F. D. Fischer, and O. Kolednik, "Hindered crack propagation in materials with periodically varying Young's Modulus—lessons from biological materials," *Advanced Materials*, vol. 19, no. 18, pp. 2657–2661, 2007.

[53] M. R. Murshed, S. I. Ranganathan, and F. H. Abed, "Design maps for fracture resistant functionally graded materials," *European Journal of Mechanics - A/Solids*, vol. 58, pp. 31–41, 2016. [Online]. Available: http://www.sciencedirect.com/science/article/pii/S0997753816000036

[54] T. L. Anderson, *Fracture mechanics: fundamentals and applications*. CRC press, 2005.

[55] R. S. Barsoum, "On the use of isoparametric finite elements in linear fracture mechanics," *International Journal for Numerical Methods in Engineering*, vol. 10, no. 1, pp. 25–37, 1976.

[56] J. Chen, L. Z. Wu, and S. Y. Du, "Element-free Galerkin methods for fracture of functionally-graded materials," *Key Engineering Materials*, vol. 183, pp. 487–492, 2000.

[57] Z.-H. Jin and G. H. Paulino, "A viscoelastic functionally graded strip containing a crack subjected to in-plane loading," *Engineering Fracture Mechanics*, vol. 69, no. 14, pp. 1769–1790, 2002.

[58] N.-A. Noda and X. Lan, "Stress intensity factors for an edge interface crack in a bonded semi-infinite plate for arbitrary material combination," *International Journal of Solids and Structures*, vol. 49, no. 10, pp. 1241–1251, 2012.

[59] M. R. Murshed, S. I. Ranganathan, and F. H. Abed, "Effect of material contrast and crack length on the fracture of functionally graded materials," *Mach Conference*, Annapolis, MD, USA, 2015.